HOGgles: Visualizing Object Detection Features*

Carl Vondrick, Aditya Khosla, Tomasz Malisiewicz, Antonio Torralba
Massachusetts Institute of Technology
{vondrick,khosla,tomasz,torralba}@csail.mit.edu

Abstract

We introduce algorithms to visualize feature spaces used by object detectors. The tools in this paper allow a human to put on 'HOG goggles' and perceive the visual world as a HOG based object detector sees it. We found that these visualizations allow us to analyze object detection systems in new ways and gain new insight into the detector's failures. For example, when we visualize the features for high scoring false alarms, we discovered that, although they are clearly wrong in image space, they do look deceptively similar to true positives in feature space. This result suggests that many of these false alarms are caused by our choice of feature space, and indicates that creating a better learning algorithm or building bigger datasets is unlikely to correct these errors. By visualizing feature spaces, we can gain a more intuitive understanding of our detection systems.

1. Introduction

Figure 1 shows a high scoring detection from an object detector with HOG features and a linear SVM classifier trained on PASCAL. Despite our field's incredible progress in object recognition over the last decade, *why* do our detectors still think that sea water looks like a car?

Unfortunately, computer vision researchers are often unable to explain the failures of object detection systems. Some researchers blame the features, others the training set, and even more the learning algorithm. Yet, if we wish to build the next generation of object detectors, it seems crucial to understand the failures of our current detectors.

In this paper, we introduce a tool to explain some of the failures of object detection systems.[1] We present algorithms to visualize the feature spaces of object detectors. Since features are too high dimensional for humans to directly inspect, our visualization algorithms work by inverting features back to natural images. We found that these inversions provide an intuitive and accurate visualization of the feature spaces used by object detectors.

*Previously: Inverting and Visualizing Features for Object Detection

[1] Code is available online at http://mit.edu/vondrick/ihog

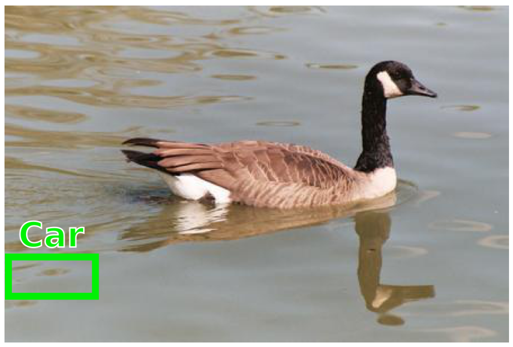

Figure 1: An image from PASCAL and a high scoring car detection from DPM [8]. Why did the detector fail?

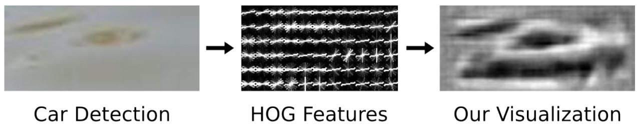

Figure 2: We show the crop for the false car detection from Figure 1. On the right, we show our visualization of the HOG features for the same patch. Our visualization reveals that this false alarm actually looks like a car in HOG space.

Figure 2 shows the output from our visualization on the features for the false car detection. This visualization reveals that, while there are clearly no cars in the original image, there is a car hiding in the HOG descriptor. HOG features see a slightly different visual world than what we see, and by visualizing this space, we can gain a more intuitive understanding of our object detectors.

Figure 3 inverts more top detections on PASCAL for a few categories. Can you guess which are false alarms? Take a minute to study the figure since the next sentence might ruin the surprise. Although every visualization looks like a true positive, all of these detections are actually false alarms. Consequently, even with a better learning algorithm or more data, these false alarms will likely persist. In other words, the features are to blame.

The principle contribution of this paper is the presentation of algorithms for visualizing features used in object detection. To this end, we present four algorithms to invert

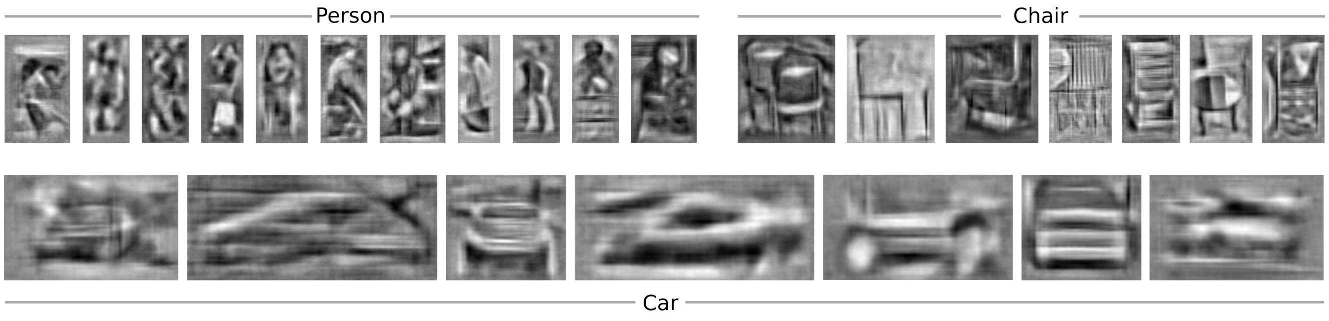

Figure 3: We visualize some high scoring detections from the deformable parts model [8] for person, chair, and car. Can you guess which are false alarms? Take a minute to study this figure, then see Figure 16 for the corresponding RGB patches.

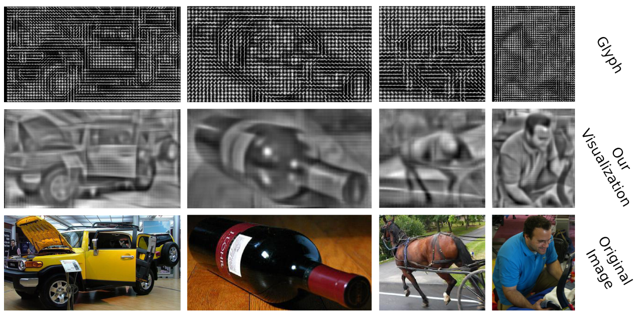

Figure 4: In this paper, we present algorithms to visualize HOG features. Our visualizations are perceptually intuitive for humans to understand.

object detection features to natural images. Although we focus on HOG features in this paper, our approach is general and can be applied to other features as well. We evaluate our inversions with both automatic benchmarks and a large human study, and we found our visualizations are perceptually more accurate at representing the content of a HOG feature than existing methods; see Figure 4 for a comparison between our visualization and HOG glyphs. We then use our visualizations to inspect the behaviors of object detection systems and analyze their features. Since we hope our visualizations will be useful to other researchers, our final contribution is a public feature visualization toolbox.

2. Related Work

Our visualization algorithms extend an actively growing body of work in feature inversion. Torralba and Oliva, in early work, described a simple iterative procedure to recover images only given gist descriptors [17]. Weinzaepfel et al. [22] were the first to reconstruct an image given its keypoint SIFT descriptors [13]. Their approach obtains compelling reconstructions using a nearest neighbor based approach on a massive database. d'Angelo et al. [4] then developed an algorithm to reconstruct images given only LBP features [2, 1]. Their method analytically solves for the inverse image and does not require a dataset.

While [22, 4, 17] do a good job at reconstructing images from SIFT, LBP, and gist features, our visualization algorithms have several advantages. Firstly, while existing methods are tailored for specific features, our visualization algorithms we propose are feature independent. Since we cast feature inversion as a machine learning problem, our algorithms can be used to visualize any feature. In this paper, we focus on features for object detection, the most popular of which is HOG. Secondly, our algorithms are fast: our best algorithm can invert features in under a second on a desktop computer, enabling interactive visualization. Finally, to our knowledge, this paper is the first to invert HOG.

Our visualizations enable analysis that complement a recent line of papers that provide tools to diagnose object recognition systems, which we briefly review here. Parikh and Zitnick [18, 19] introduced a new paradigm for human debugging of object detectors, an idea that we adopt in our experiments. Hoiem et al. [10] performed a large study analyzing the errors that object detectors make. Divvala et al. [5] analyze part-based detectors to determine which components of object detection systems have the most impact on performance. Tatu et al. [20] explored the set of images that generate identical HOG descriptors. Liu and Wang [12] designed algorithms to highlight which image regions contribute the most to a classifier's confidence. Zhu et al. [24] try to determine whether we have reached Bayes risk for HOG. The tools in this paper enable an alternative mode to analyze object detectors through visualizations. By putting on 'HOG glasses' and visualizing the world according to the features, we are able to gain a better understanding of the failures and behaviors of our object detection systems.

3. Feature Visualization Algorithms

We pose the feature visualization problem as one of feature inversion, i.e. recovering the natural image that generated a feature vector. Let $x \in \mathbb{R}^D$ be an image and $y = \phi(x)$ be the corresponding HOG feature descriptor. Since $\phi(\cdot)$ is a many-to-one function, no analytic inverse exists. Hence, we seek an image x that, when we compute

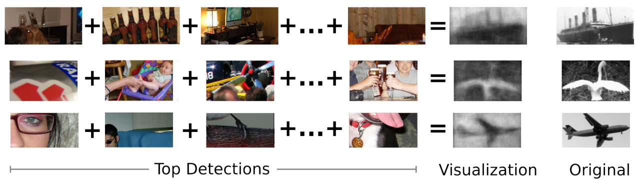

Figure 5: We found that averaging the images of top detections from an exemplar LDA detector provide one method to invert HOG features.

HOG on it, closely matches the original descriptor y:

$$\phi^{-1}(y) = \operatorname*{argmin}_{x \in \mathbb{R}^D} ||\phi(x) - y||_2^2 \tag{1}$$

Optimizing Eqn.1 is challenging. Although Eqn.1 is not convex, we tried gradient-descent strategies by numerically evaluating the derivative in image space with Newton's method. Unfortunately, we observed poor results, likely because HOG is both highly sensitive to noise and Eqn.1 has frequent local minima.

In the rest of this section, we present four algorithms for inverting HOG features. Since, to our knowledge, no algorithms to invert HOG have yet been developed, we first describe three simple baselines for HOG inversion. We then present our main inversion algorithm.

3.1. Baseline A: Exemplar LDA (ELDA)

Consider the top detections for the exemplar object detector [9, 15] for a few images shown in Figure 5. Although all top detections are false positives, notice that each detection captures some statistics about the query. Even though the detections are wrong, if we squint, we can see parts of the original object appear in each detection.

We use this simple observation to produce our first inversion baseline. Suppose we wish to invert HOG feature y. We first train an exemplar LDA detector [9] for this query, $w = \Sigma^{-1}(y - \mu)$. We score w against every sliding window on a large database. The HOG inverse is then the average of the top K detections in RGB space: $\phi_A^{-1}(y) = \frac{1}{K}\sum_{i=1}^{K} z_i$ where z_i is an image of a top detection.

This method, although simple, produces surprisingly accurate reconstructions, even when the database does not contain the category of the HOG template. However, it is computationally expensive since it requires running an object detector across a large database. We also point out that a similar nearest neighbor method is used in brain research to visualize what a person might be seeing [16].

3.2. Baseline B: Ridge Regression

We present a fast, parametric inversion baseline based off ridge regression. Let $X \in \mathbb{R}^D$ be a random variable representing a gray scale image and $Y \in \mathbb{R}^d$ be a random variable of its corresponding HOG point. We define these random variables to be normally distributed on a $D + d$-variate Gaussian $P(X, Y) \sim \mathcal{N}(\mu, \Sigma)$ with parameters $\mu = \begin{bmatrix} \mu_X & \mu_Y \end{bmatrix}$ and $\Sigma = \begin{bmatrix} \Sigma_{XX} & \Sigma_{XY} \\ \Sigma_{XY}^T & \Sigma_{YY} \end{bmatrix}$. In order to invert a HOG feature y, we calculate the most likely image from the conditional Gaussian distribution $P(X|Y = y)$:

$$\phi_B^{-1}(y) = \operatorname*{argmax}_{x \in \mathbb{R}^D} P(X = x|Y = y) \tag{2}$$

It is well known that Gaussians have a closed form conditional mode:

$$\phi_B^{-1}(y) = \Sigma_{XY}\Sigma_{YY}^{-1}(y - \mu_Y) + \mu_X \tag{3}$$

Under this inversion algorithm, any HOG point can be inverted by a single matrix multiplication, allowing for inversion in under a second.

We estimate μ and Σ on a large database. In practice, Σ is not positive definite; we add a small uniform prior (i.e., $\hat{\Sigma} = \Sigma + \lambda I$) so Σ can be inverted. Since we wish to invert any HOG point, we assume that $P(X, Y)$ is stationary [9], allowing us to efficiently learn the covariance across massive datasets. We invert an arbitrary dimensional HOG point by marginalizing out unused dimensions.

We found that ridge regression yields blurred inversions. Intuitively, since HOG is invariant to shifts up to its bin size, there are many images that map to the same HOG point. Ridge regression is reporting the statistically most likely image, which is the average over all shifts. This causes ridge regression to only recover the low frequencies of the original image.

3.3. Baseline C: Direct Optimization

We now provide a baseline that attempts to find images that, when we compute HOG on it, sufficiently match the original descriptor. In order to do this efficiently, we only consider images that span a natural image basis. Let $U \in \mathbb{R}^{D \times K}$ be the natural image basis. We found using the first K eigenvectors of $\Sigma_{XX} \in \mathbb{R}^{D \times D}$ worked well for this basis. Any image $x \in \mathbb{R}^D$ can be encoded by coefficients $\rho \in \mathbb{R}^K$ in this basis: $x = U\rho$. We wish to minimize:

$$\begin{aligned} &\phi_C^{-1}(y) = U\rho^* \\ &\text{where} \quad \rho^* = \operatorname*{argmin}_{\rho \in \mathbb{R}^K} ||\phi(U\rho) - y||_2^2 \end{aligned} \tag{4}$$

Empirically we found success optimizing Eqn.4 using coordinate descent on ρ with random restarts. We use an overcomplete basis corresponding to sparse Gabor-like filters for U. We compute the eigenvectors of Σ_{XX} across different scales and translate smaller eigenvectors to form U.

3.4. Algorithm D: Paired Dictionary Learning

In this section, we present our main inversion algorithm. Let $x \in \mathbb{R}^D$ be an image and $y \in \mathbb{R}^d$ be its HOG descriptor.

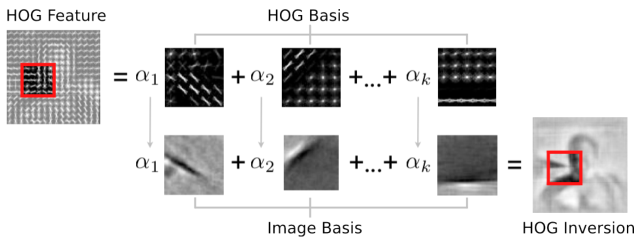

Figure 6: Inverting HOG using paired dictionary learning. We first project the HOG vector on to a HOG basis. By jointly learning a coupled basis of HOG features and natural images, we then transfer the coefficients to the image basis to recover the natural image.

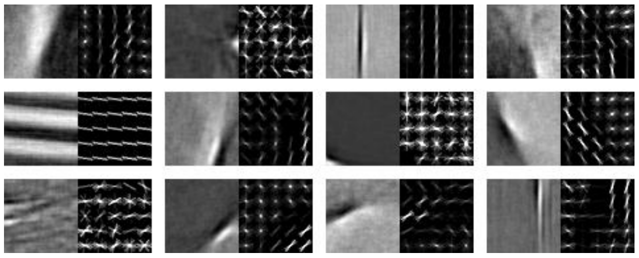

Figure 7: Some pairs of dictionaries for U and V. The left of every pair is the gray scale dictionary element and the right is the positive components elements in the HOG dictionary. Notice the correlation between dictionaries.

Suppose we write x and y in terms of bases $U \in \mathbb{R}^{D \times K}$ and $V \in \mathbb{R}^{d \times K}$ respectively, but with shared coefficients $\alpha \in \mathbb{R}^K$:

$$x = U\alpha \quad \text{and} \quad y = V\alpha \tag{5}$$

The key observation is that inversion can be obtained by first projecting the HOG features y onto the HOG basis V, then projecting α into the natural image basis U:

$$\begin{aligned} &\phi_D^{-1}(y) = U\alpha^* \\ &\text{where} \quad \alpha^* = \underset{\alpha \in \mathbb{R}^K}{\operatorname{argmin}} \, ||V\alpha - y||_2^2 \quad \text{s.t.} \quad ||\alpha||_1 \leq \lambda \end{aligned} \tag{6}$$

See Figure 6 for a graphical representation of the paired dictionaries. Since efficient solvers for Eqn.6 exist [14, 11], we can invert features in under two seconds on a 4 core CPU.

Paired dictionaries require finding appropriate bases U and V such that Eqn.5 holds. To do this, we solve a paired dictionary learning problem, inspired by recent super resolution sparse coding work [23, 21]:

$$\begin{aligned} &\underset{U,V,\alpha}{\operatorname{argmin}} \sum_{i=1}^{N} \left(||x_i - U\alpha_i||_2^2 + ||\phi(x_i) - V\alpha_i||_2^2 \right) \\ &\quad \text{s.t.} \quad ||\alpha_i||_1 \leq \lambda \; \forall i, \; ||U||_2^2 \leq \gamma_1, \; ||V||_2^2 \leq \gamma_2 \end{aligned} \tag{7}$$

After a few algebraic manipulations, the above objective simplifies to a standard sparse coding and dictionary learning problem with concatenated dictionaries, which we optimize using SPAMS [14]. Optimization typically took a few hours on medium sized problems. We estimate U and V with a dictionary size $K \approx 10^3$ and training samples $N \approx 10^6$ from a large database. See Figure 7 for a visualization of the learned dictionary pairs.

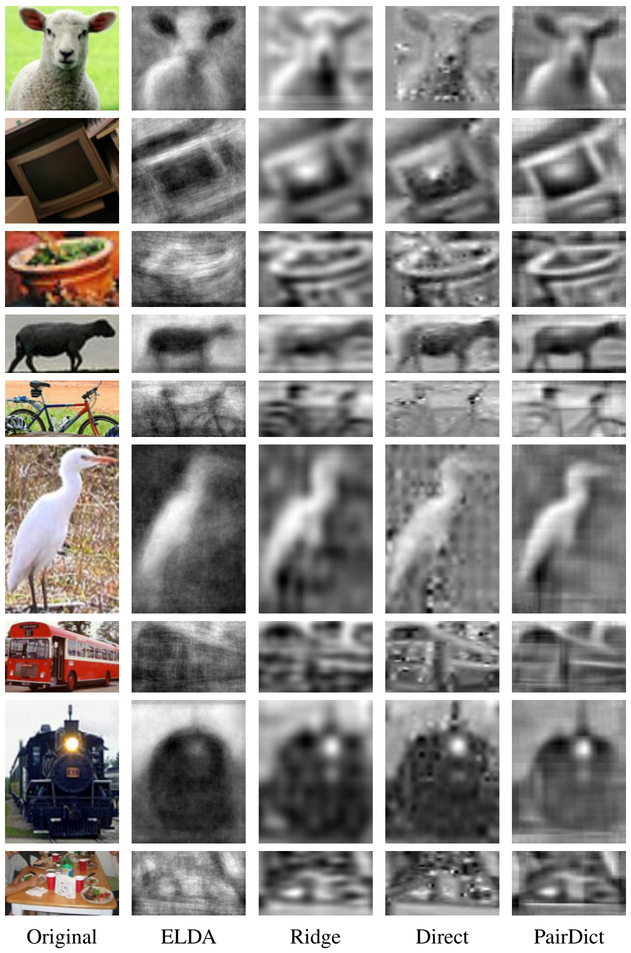

Figure 8: We show results for all four of our inversion algorithms on held out image patches on similar dimensions common for object detection. See supplemental for more.

4. Evaluation of Visualizations

We evaluate our inversion algorithms using both qualitative and quantitative measures. We use PASCAL VOC 2011 [6] as our dataset and we invert patches corresponding to objects. Any algorithm that required training could only access the training set. During evaluation, only images from the validation set are examined. The database for exemplar LDA excluded the category of the patch we were inverting to reduce the potential effect of dataset biases.

We show our inversions in Figure 8 for a few object categories. Exemplar LDA and ridge regression tend to pro-

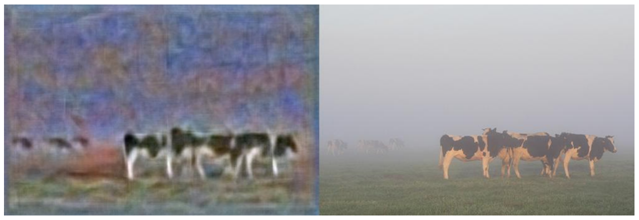

Figure 9: We show results where our paired dictionary algorithm is trained to recover RGB images instead of only grayscale images. The right shows the original image and the left shows the inverse.

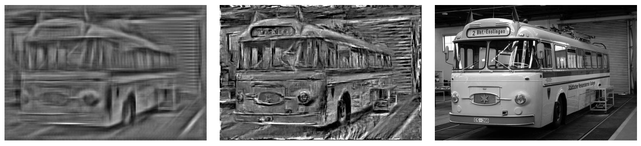

Figure 10: Although our algorithms are good at inverting HOG, they are not perfect, and struggle to reconstruct high frequency detail. See text for details.

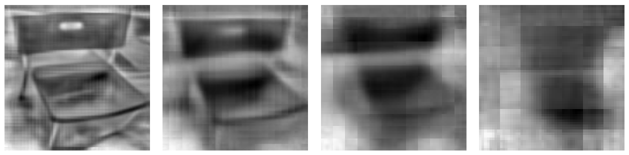

Figure 11: Our inversion algorithms are sensitive to the HOG template size. We show how performance degrades as the template becomes smaller.

duce blurred visualizations. Direct optimization recovers high frequency details at the expense of extra noise. Paired dictionary learning tends to produce the best visualization for HOG descriptors. By learning a dictionary over the visual world and the correlation between HOG and natural images, paired dictionary learning recovered high frequencies without introducing significant noise.

We discovered that the paired dictionary is able to recover color from HOG descriptors. Figure 9 shows the result of training a paired dictionary to estimate RGB images instead of grayscale images. While the paired dictionary assigns arbitrary colors to man-made objects and in-door scenes, it frequently colors natural objects correctly, such as grass or the sky, likely because those categories are strongly correlated to HOG descriptors. We focus on grayscale visualizations in this paper because we found those to be more intuitive for humans to understand.

While our visualizations do a good job at representing HOG features, they have some limitations. Figure 10 compares our best visualization (paired dictionary) against a greedy algorithm that draws triangles of random rotation, scale, position, and intensity, and only accepts the triangle if it improves the reconstruction. If we allow the greedy al-

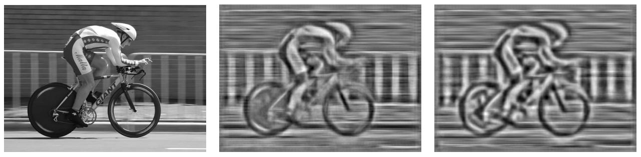

Figure 12: We recursively compute HOG and invert it with a paired dictionary. While there is some information loss, our visualizations still do a good job at accurately representing HOG features. $\phi(\cdot)$ is HOG, and $\phi^{-1}(\cdot)$ is the inverse.

gorithm to execute for an extremely long time (a few days), the visualization better shows higher frequency detail. This reveals that there exists a visualization better than paired dictionary learning, although it may not be tractable. In a related experiment, Figure 12 recursively computes HOG on the inverse and inverts it again. This recursion shows that there is some loss between iterations, although it is minor and appears to discard high frequency details. Moreover, Figure 11 indicates that our inversions are sensitive to the dimensionality of the HOG template. Despite these limitations, our visualizations are, as we will now show, still perceptually intuitive for humans to understand.

We quantitatively evaluate our algorithms under two benchmarks. Firstly, we use an automatic inversion metric that measures how well our inversions reconstruct original images. Secondly, we conducted a large visualization challenge with human subjects on Amazon Mechanical Turk (MTurk), which is designed to determine how well people can infer high level semantics from our visualizations.

4.1. Inversion Benchmark

We consider the inversion performance of our algorithm: given a HOG feature y, how well does our inverse $\phi^{-1}(y)$ reconstruct the original pixels x for each algorithm? Since HOG is invariant up to a constant shift and scale, we score each inversion against the original image with normalized cross correlation. Our results are shown in Table 1. Overall, exemplar LDA does the best at pixel level reconstruction.

4.2. Visualization Benchmark

While the inversion benchmark evaluates how well the inversions reconstruct the original image, it does not capture the high level content of the inverse: is the inverse of a sheep still a sheep? To evaluate this, we conducted a study on MTurk. We sampled 2,000 windows corresponding to objects in PASCAL VOC 2011. We then showed participants an inversion from one of our algorithms and asked users to classify it into one of the 20 categories. Each window was shown to three different users. Users were required to pass a training course and qualification exam before participating in order to guarantee users understood the task. Users could optionally select that they were not confident in

Category	ELDA	Ridge	Direct	PairDict
bicycle	0.452	**0.577**	0.513	0.561
bottle	**0.697**	0.683	0.660	0.671
car	0.668	**0.677**	0.652	0.639
cat	**0.749**	0.712	0.687	0.705
chair	**0.660**	0.621	0.604	0.617
table	**0.656**	0.617	0.582	0.614
motorbike	0.573	**0.617**	0.549	0.592
person	**0.696**	0.667	0.646	0.646
Mean	**0.671**	0.656	0.620	0.637

Table 1: We evaluate the performance of our inversion algorithm by comparing the inverse to the ground truth image using the mean normalized cross correlation. Higher is better; a score of 1 is perfect. See supplemental for full table.

Category	ELDA	Ridge	Direct	PairDict	Glyph	Expert
bicycle	0.327	0.127	0.362	0.307	**0.405**	0.438
bottle	0.269	0.282	0.283	**0.446**	0.312	0.222
car	0.397	0.457	**0.617**	0.585	0.359	0.389
cat	0.219	0.178	**0.381**	0.199	0.139	0.286
chair	0.099	0.239	0.223	**0.386**	0.119	0.167
table	0.152	0.064	0.162	**0.237**	0.071	0.125
motorbike	0.221	0.232	**0.396**	0.224	0.298	0.350
person	0.458	0.546	0.502	**0.676**	0.301	0.375
Mean	0.282	0.258	0.355	**0.383**	0.191	0.233

Table 2: We evaluate visualization performance across twenty PASCAL VOC categories by asking MTurk workers to classify our inversions. Numbers are percent classified correctly; higher is better. Chance is 0.05. Glyph refers to the standard black-and-white HOG diagram popularized by [3]. Paired dictionary learning provides the best visualizations for humans. Expert refers to MIT PhD students in computer vision performing the same visualization challenge with HOG glyphs. See supplemental for full table.

their answer. We also compared our algorithms against the standard black-and-white HOG glyph popularized by [3].

Our results in Table 2 show that paired dictionary learning and direct optimization provide the best visualization of HOG descriptors for humans. Ridge regression and exemplar LDA performs better than the glyph, but they suffer from blurred inversions. Human performance on the HOG glyph is generally poor, and participants were even the slowest at completing that study. Interestingly, the glyph does the best job at visualizing bicycles, likely due to their unique circular gradients. Our results overall suggest that visualizing HOG with the glyph is misleading, and richer visualizations from our paired dictionary are useful for interpreting HOG vectors.

Our experiments suggest that humans can predict the performance of object detectors by only looking at HOG visualizations. Human accuracy on inversions and state-of-the-art object detection AP scores from [7] are correlated with a Spearman's rank correlation coefficient of 0.77.

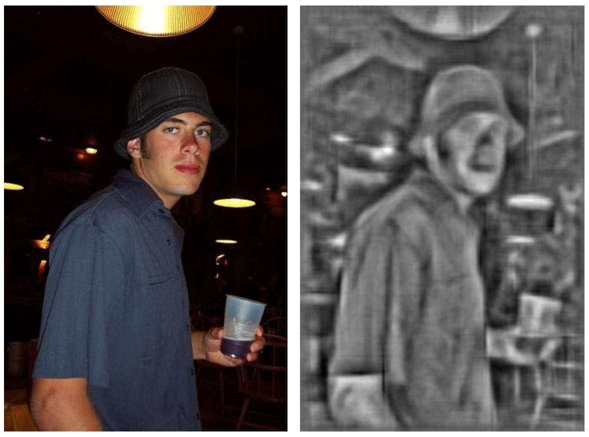
(a) Human Vision (b) HOG Vision

Figure 13: HOG inversion reveals the world that object detectors see. The left shows a man standing in a dark room. If we compute HOG on this image and invert it, the previously dark scene behind the man emerges. Notice the wall structure, the lamp post, and the chair in the bottom right hand corner.

We also asked computer vision PhD students at MIT to classify HOG glyphs in order to compare MTurk workers with experts in HOG. Our results are summarized in the last column of Table 2. HOG experts performed slightly better than non-experts on the glyph challenge, but experts on glyphs did not beat non-experts on other visualizations. This result suggests that our algorithms produce more intuitive visualizations even for object detection researchers.

5. Understanding Object Detectors

We have so far presented four algorithms to visualize object detection features. We evaluated the visualizations with a large human study, and we found that paired dictionary learning provides the most intuitive visualization of HOG features. In this section, we will use this visualization to inspect the behavior of object detection systems.

5.1. HOG Goggles

Our visualizations reveal that the world that features see is slightly different from the world that the human eye perceives. Figure 13a shows a normal photograph of a man standing in a dark room, but Figure 13b shows how HOG features see the same man. Since HOG is invariant to illumination changes and amplifies gradients, the background of the scene, normally invisible to the human eye, materializes in our visualization.

In order to understand how this clutter affects object detection, we visualized the features of some of the top false alarms from the Felzenszwalb et al. object detection system [8] when applied to the PASCAL VOC 2007 test set.

Figure 3 shows our visualizations of the features of the top false alarms. Notice how the false alarms look very similar to true positives. While there are many different types of detector errors, this result suggests that these particular failures are due to limitations of HOG, and consequently, even if we develop better learning algorithms or use larger datasets, these will false alarms will likely persist.

Figure 16 shows the corresponding RGB image patches for the false positives discussed above. Notice how when we view these detections in image space, all of the false alarms are difficult to explain. Why do chair detectors fire on buses, or people detectors on cherries? By visualizing the detections in feature space, we discovered that the learning algorithm made reasonable failures since the features are deceptively similar to true positives.

5.2. Human+HOG Detectors

Although HOG features are designed for machines, how well do humans see in HOG space? If we could quantify human vision on the HOG feature space, we could get insights into the performance of HOG with a perfect learning algorithm (people). Inspired by Parikh and Zitnick's methodology [18, 19], we conducted a large human study where we had Amazon Mechanical Turk workers act as sliding window HOG based object detectors.

We built an online interface for humans to look at HOG visualizations of window patches at the same resolution as DPM. We instructed workers to either classify a HOG visualization as a positive example or a negative example for a category. By averaging over multiple people (we used 25 people per window), we obtain a real value score for a HOG patch. To build our dataset, we sampled top detections from DPM on the PASCAL VOC 2007 dataset for a few categories. Our dataset consisted of around $5,000$ windows per category and around 20% were true positives.

Figure 14 shows precision recall curves for the Human+HOG based object detector. In most cases, human subjects classifying HOG visualizations were able to rank sliding windows with either the same accuracy or better than DPM. Humans tied DPM for recognizing cars, suggesting that performance may be saturated for car detection on HOG. Humans were slightly superior to DPM for chairs, although performance might be nearing saturation soon. There appears to be the most potential for improvement for detecting cats with HOG. Subjects performed slightly worst than DPM for detecting people, but we believe this is the case because humans tend to be good at fabricating people in abstract drawings.

We then repeated the same experiment as above on chairs except we instructed users to classify the original RGB patch instead of the HOG visualization. As expected, humans achieved near perfect accuracy at detecting chairs with RGB sliding windows. The performance gap between the Human+HOG detector and Human+RGB detector demonstrates the amount of information that HOG features discard.

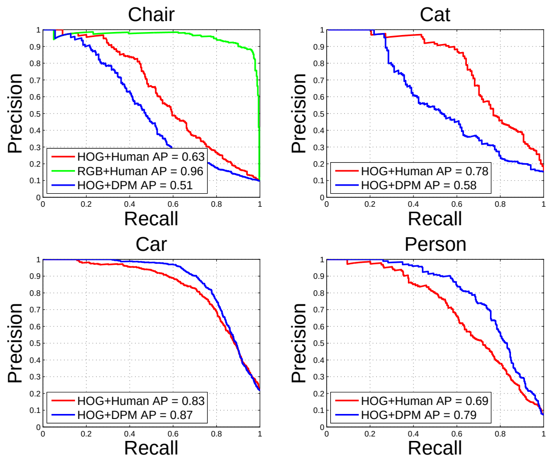

Figure 14: By instructing multiple human subjects to classify the visualizations, we show performance results with an ideal learning algorithm (i.e., humans) on the HOG feature space. Please see text for details.

Our experiments suggest that there is still some performance left to be squeezed out of HOG. However, DPM is likely operating very close to the performance limit of HOG. Since humans are the ideal learning agent and they still had trouble detecting objects in HOG space, HOG may be too lossy of a descriptor for high performance object detection. If we wish to significantly advance the state-of-the-art in recognition, we suspect focusing effort on building better features that capture finer details as well as higher level information will lead to substantial performance improvements in object detection.

5.3. Model Visualization

We found our algorithms are also useful for visualizing the learned models of an object detector. Figure 15 visualizes the root templates and the parts from [8] by inverting the positive components of the learned weights. These visualizations provide hints on which gradients the learning found discriminative. Notice the detailed structure that emerges from our visualization that is not apparent in the HOG glyph. In most cases, one can recognize the category of the detector by only looking at the visualizations.

6. Conclusion

We believe visualizations can be a powerful tool for understanding object detection systems and advancing research in computer vision. To this end, this paper presented and evaluated four algorithms to visualize object detection features. Since object detection researchers analyze HOG glyphs everyday and nearly every recent object detection

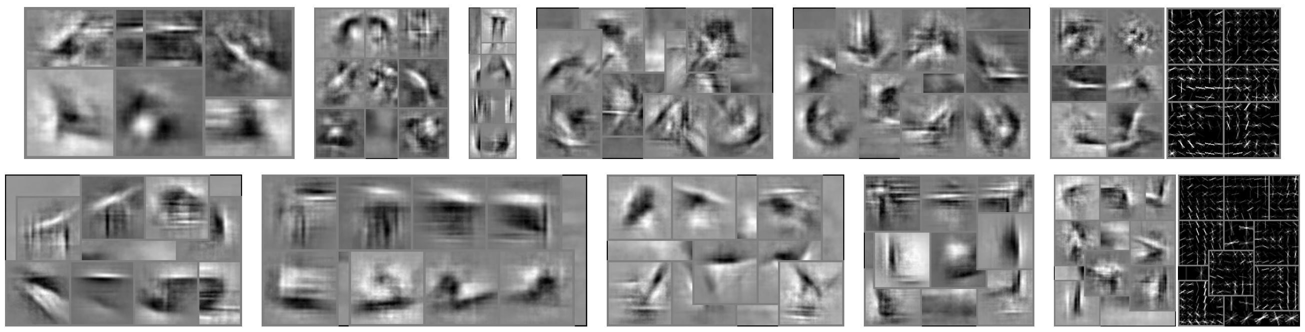

Figure 15: We visualize a few deformable parts models trained with [8]. Notice the structure that emerges with our visualization. First row: car, person, bottle, bicycle, motorbike, potted plant. Second row: train, bus, horse, television, chair. For the right most visualizations, we also included the HOG glyph. Our visualizations tend to reveal more detail than the glyph.

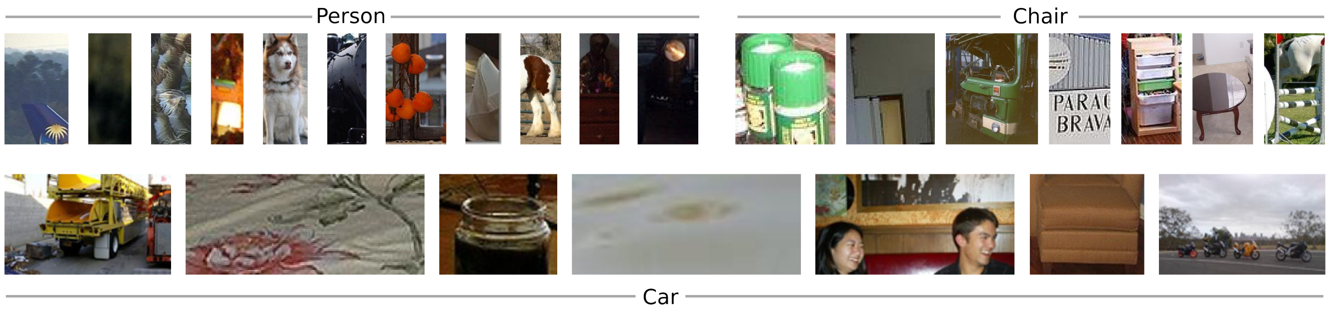

Figure 16: We show the original RGB patches that correspond to the visualizations from Figure 3. We print the original patches on a separate page to highlight how the inverses of false positives look like true positives. We recommend comparing this figure side-by-side with Figure 3.

paper includes HOG visualizations, we hope more intuitive visualizations will prove useful for the community.

Acknowledgments: We thank Hamed Pirsiavash, Joseph Lim, MIT CSAIL Vision Group, and reviewers. Funding was provided by a NSF GRFP to CV, a Facebook fellowship to AK, and a Google research award, ONR MURI N000141010933 and NSF Career Award No. 0747120 to AT.

References

[1] A. Alahi, R. Ortiz, and P. Vandergheynst. Freak: Fast retina keypoint. In *CVPR*, 2012. 2

[2] M. Calonder, V. Lepetit, C. Strecha, and P. Fua. Brief: Binary robust independent elementary features. *ECCV*, 2010. 2

[3] N. Dalal and B. Triggs. Histograms of oriented gradients for human detection. In *CVPR*, 2005. 6

[4] E. d'Angelo, A. Alahi, and P. Vandergheynst. Beyond bits: Reconstructing images from local binary descriptors. *ICPR*, 2012. 2

[5] S. Divvala, A. Efros, and M. Hebert. How important are deformable parts in the deformable parts model? *Technical Report*, 2012. 2

[6] M. Everingham, L. Van Gool, C. K. I. Williams, J. Winn, and A. Zisserman. The pascal visual object classes challenge. *IJCV*, 2010. 4

[7] P. Felzenszwalb, R. Girshick, and D. McAllester. Cascade object detection with deformable part models. In *CVPR*, 2010. 6

[8] P. Felzenszwalb, R. Girshick, D. McAllester, and D. Ramanan. Object detection with discriminatively trained part-based models. *PAMI*, 2010. 1, 2, 6, 7, 8

[9] B. Hariharan, J. Malik, and D. Ramanan. Discriminative decorrelation for clustering and classification. *ECCV*, 2012. 3

[10] D. Hoiem, Y. Chodpathumwan, and Q. Dai. Diagnosing error in object detectors. *ECCV*, 2012. 2

[11] H. Lee, A. Battle, R. Raina, and A. Ng. Efficient sparse coding algorithms. *NIPS*, 2007. 4

[12] L. Liu and L. Wang. What has my classifier learned? visualizing the classification rules of bag-of-feature model by support region detection. In *CVPR*, 2012. 2

[13] D. Lowe. Object recognition from local scale-invariant features. In *ICCV*, 1999. 2

[14] J. Mairal, F. Bach, J. Ponce, and G. Sapiro. Online dictionary learning for sparse coding. In *ICML*, 2009. 4

[15] T. Malisiewicz, A. Gupta, and A. Efros. Ensemble of exemplar-svms for object detection and beyond. In *ICCV*, 2011. 3

[16] S. Nishimoto, A. Vu, T. Naselaris, Y. Benjamini, B. Yu, and J. Gallant. Reconstructing visual experiences from brain activity evoked by natural movies. *Current Biology*, 2011. 3

[17] A. Oliva and A. Torralba. Modeling the shape of the scene: A holistic representation of the spatial envelope. *IJCV*, 2001. 2

[18] D. Parikh and C. Zitnick. Human-debugging of machines. In *NIPS WCSSWC*, 2011. 2, 7

[19] D. Parikh and C. L. Zitnick. The role of features, algorithms and data in visual recognition. In *CVPR*, 2010. 2, 7

[20] A. Tatu, F. Lauze, M. Nielsen, and B. Kimia. Exploring the representation capabilities of hog descriptors. In *ICCV WIT*, 2011. 2

[21] S. Wang, L. Zhang, Y. Liang, and Q. Pan. Semi-coupled dictionary learning with applications to image super-resolution and photo-sketch synthesis. In *CVPR*, 2012. 4

[22] P. Weinzaepfel, H. Jégou, and P. Pérez. Reconstructing an image from its local descriptors. In *CVPR*, 2011. 2

[23] J. Yang, J. Wright, T. Huang, and Y. Ma. Image super-resolution via sparse representation. *Transactions on Image Processing*, 2010. 4

[24] X. Zhu, C. Vondrick, D. Ramanan, and C. Fowlkes. Do we need more training data or better models for object detection? *BMVC*, 2012. 2

A. Full Evaluation Tables

We provide the full inversion benchmark with normalized cross correlation:

Category	ELDA	Ridge	Direct	PairDict
aeroplane	**0.634**	**0.633**	0.596	0.609
bicycle	0.452	**0.577**	0.513	0.561
bird	**0.680**	0.650	0.618	0.638
boat	**0.697**	0.678	0.631	0.629
bottle	**0.697**	0.683	0.660	0.671
bus	0.627	**0.632**	0.587	0.585
car	0.668	**0.677**	0.652	0.639
cat	**0.749**	0.712	0.687	0.705
chair	**0.660**	0.621	0.604	0.617
cow	**0.720**	0.663	0.632	0.650
table	**0.656**	0.617	0.582	0.614
dog	**0.717**	0.676	0.638	0.667
horse	**0.686**	0.633	0.586	0.635
motorbike	0.573	**0.617**	0.549	0.592
person	**0.696**	0.667	0.646	0.646
pottedplant	**0.674**	**0.679**	0.629	0.649
sheep	**0.743**	0.731	0.692	0.695
sofa	**0.691**	0.657	0.633	0.657
train	**0.697**	0.684	0.634	0.645
tvmonitor	**0.711**	0.640	0.638	0.629
Mean	**0.671**	0.656	0.620	0.637

We provide the full visualization benchmark with human subjects:

Category	ELDA	Ridge	Direct	PairDict	Glyph	Expert
aeroplane	0.433	0.391	0.568	**0.645**	0.297	0.333
bicycle	0.327	0.127	0.362	0.307	**0.405**	0.438
bird	0.364	0.263	**0.378**	0.372	0.193	0.059
boat	0.292	0.182	0.255	**0.329**	0.119	0.352
bottle	0.269	0.282	0.283	**0.446**	0.312	0.222
bus	0.473	0.395	**0.541**	**0.549**	0.122	0.118
car	0.397	0.457	**0.617**	0.585	0.359	0.389
cat	0.219	0.178	**0.381**	0.199	0.139	0.286
chair	0.099	0.239	0.223	**0.386**	0.119	0.167
cow	0.133	0.103	**0.230**	0.197	0.072	0.214
table	0.152	0.064	0.162	**0.237**	0.071	0.125
dog	0.222	0.316	**0.351**	0.343	0.107	0.150
horse	0.260	0.290	0.354	**0.446**	0.144	0.150
motorbike	0.221	0.232	**0.396**	0.224	0.298	0.350
person	0.458	0.546	0.502	**0.676**	0.301	0.375
pottedplant	0.112	0.109	**0.203**	0.091	0.080	0.136
sheep	0.227	0.194	**0.368**	0.253	0.041	0.000
sofa	0.138	0.100	0.162	**0.293**	0.104	0.000
train	0.311	0.244	0.316	**0.404**	0.173	0.133
tvmonitor	0.537	0.439	0.449	**0.682**	0.354	0.666
Mean	0.282	0.258	0.355	**0.383**	0.191	0.233

B. Visualization Class Confusions

We show the confusion matrices for humans classifying our HOG inversions for various algorithms:

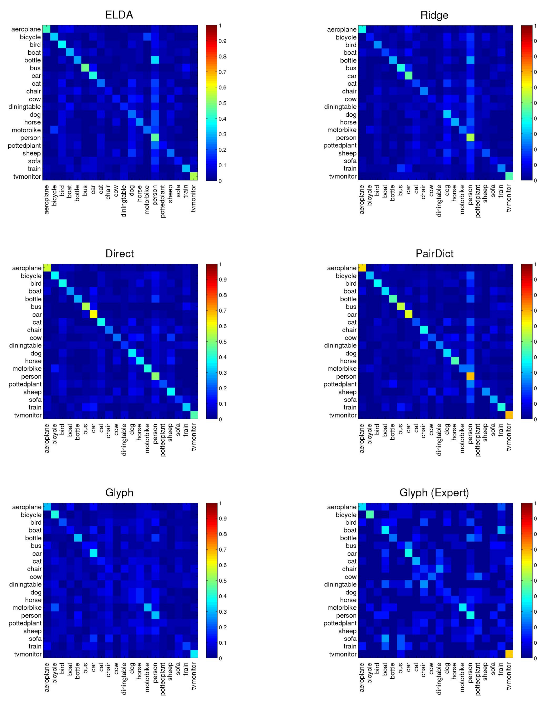

C. Additional Color Inversions

On the left, we show the color inverse. On the right, we show the original image.